Available online at www.sciencedirect.com
SCIENCE DIRECT
Journal of Organometallic Chemistry 691 (2006) 869–878
Journal of Organometallic Chemistry
www.elsevier.com/locate/jorganchem

Search of structure and ligands exchange for palladium(II) complexes with *N*-allylimidazole; X-ray and solid-state/solution NMR studies

Krystyna Kurdziel [a], Sebastian Olejniczak [b], Andrzej Okruszek [b,c], Tadeusz Głowiak [d], Rafał Kruszyński [e], Stefano Materazzi [f], Marek J. Potrzebowski [b,*]

[a] *Institute of Chemistry, Świętokrzyska Academy, Chęcińska 5, 25-020 Kielce, Poland*
[b] *Department of Structural Studies, Centre of Molecular and Macromolecular Studies, Polish Academy of Sciences, Sienkiewicza 112, 90-363 Łódź, Poland*
[c] *Institute of Technical Biochemistry, Technical University of Łódź, PL-90924 Łódź, Poland*
[d] *Faculty of Chemistry, Wrocław University, F. Joliot-Curie 14, 50-386 Wrocław, Poland*
[e] *X-ray Crystallography and Crystal Chemistry Group, Institute of General and Ecological Chemistry, Technical University of Łódź, PL-90924 Łódź, Poland*
[f] *Department of Chemistry, University of Rome "La Sapienza", A. Moro 5, 00185 Rome, Italy*

Received 29 July 2005; received in revised form 25 October 2005; accepted 25 October 2005
Available online 5 December 2005

Abstract

Two coordination compounds of palladium(II) with *N*-allylimidazole (L) of the general formula $[PdL_4]Cl_2 \cdot 3H_2O$ (**1**) and *trans*-$[PdL_2Cl_2]$ (**2**) have been synthesized. The crystal and molecular structure of complexes **1** and **2** was established by single-crystal X-ray diffraction analysis. The X-ray structural data were supplemented by solid-state ^{13}C NMR measurements (CP MAS and PASS 2D). The 1D and 2D NMR studies in solution reveal that complex **1** is unstable at room temperature and undergoes reversible decomposition to **2**. The method for how to preserve a complex with four allyl-imidazole ligands in solution is shown.
© 2005 Elsevier B.V. All rights reserved.

Keywords: 2D NMR; ^{13}C solid-state NMR; DFT calculations; NMR shielding; Metal complexes

1. Introduction

In recent years, nitrogen binding ligands have received a great deal of attention due to their promising properties in applied sciences, mostly owing to high efficiency in homogenous catalysis. Togni and Venanzi [1] exhaustively discussed the relevance of N-donors in organometallic chemistry. Although, to date, a number of N-ligand derivatives have found practical applications, the search for new, more effective and/or selective species is still in progress. Such chelating bi- or terdentate N-coordinating ligands as diazabutanes [2], bis(oxazolinyl)pyrrole [3], dipyridyl amides [4] and their prospective applications have been recently reported.

Much attention was paid to palladium complexes bearing different modifications of imidazole ligands. The unique and attractive feature of this class of compound is their ability to form complexes as N and/or C carbene donors. The literature describing different structural aspects of complexes with imidazole derivatives and efficacy in catalytic processes are very rich. Palladium(II) complexes of functionalized bis(imidazolium) ligands and their interaction with carbene and pseudo η^3-allyl derivatives were reported by Cavell and co-workers [5]. Done et al. [6] have investigated *N*-methylimidazole-2-yl and *N*-methylbenzimidazole-2-yl ligands in order to determine the influence of electronic and steric factors on the reactivity at the metal centres. Reddy and Krishna have tested the usefulness of

* Corresponding author. Tel.: +48 42 68 03 240; fax: +48 42 68 47 126.
E-mail address: marekpot@bilbo.cbmm.lodz.pl (M.J. Potrzebowski).

0022-328X/$ - see front matter © 2005 Elsevier B.V. All rights reserved.
doi:10.1016/j.jorganchem.2005.10.045

N-substituted 2-(2-bromobenzimidazole) palladium derivatives as highly active catalysts for Heck reactions [7]. Welton and co-workers [8] have proved that palladium imidazole complexes are effective catalysts of Suzuki cross-coupling reactions. It is apparent from the cited report that small modification of N-subsistent of imidazole has a significant influence on the efficacy of the catalytic process. Very recently Hahn, Heidrich, Luger and Pape [9] described the unsymmetrically and symmetrically substituted *N*-allyl imidazolium bromides as effective ligands of Pd(II) complexes. In their project, the influence of N-substituents on the formation of imidazolin-2-ylides and their tendency to form a C2···Pd bond is discussed.

In our work, we wish to present results on the crystal and molecular structure of two crystalline complexes formed by *N*-allylimidazole with $PdCl_2$. The X-ray structural data are supplemented by solid-state ^{13}C NMR measurements (CP MAS and PASS-2D). The 1D and 2D NMR studies in solution clearly prove that the complex with four allyl-imidazole ligands is unstable at room temperature and undergoes a reversible decomposition to a complex with two ligands directly bonded to palladium. The method for how to preserve the complex with four allyl-imidazole ligands in solution is shown.

2. Experimental

2.1. Preparation of the complexes

2.1.1. $[PdL_4]Cl_2 \cdot 3H_2O$ (1)

Palladium(II) chloride (POCh, Gliwice, Poland, (0.177 g, 1 mmol)) was dissolved in acetone (50 ml) after acidification with a few drops of conc. HCl. To this solution, an *N*-allylimidazole (Aldrich-Europe) solution in acetone (ca. 20%) was added in small portions, with stirring on a hot water bath, to adjust the pH to ca. 10. The solution was kept overnight at room temperature. The colourless crystals of the complex were filtered, washed with absolute ether and dried under vacuum at room temperature. Elemental analysis (Perkin–Elmer 240 CHN Analyzer) was in agreement with the formula $[PdL_4]Cl_2 \cdot 3H_2O$ (Found: C, 43.4; H, 5.9; N, 16.8%. $C_{24}H_{38}Cl_2N_8O_3Pd$ requires C, 43.42; H, 5.77; N, 16.89%). The crystals were stable on storage at room temperature and on heating up to ca. 90 °C.

2.1.2. $[PdL_2Cl_2]$ (2)

This compound was obtained by controlled heating of complex **1**. Thermal decomposition of $[PdL_4]Cl_2 \cdot 3H_2O$ under dynamic conditions, at atmospheric pressure, was studied using a 951 TGA Thermogravimetric Analyzer (DuPont Instruments). Upon heating above 90 °C, the complex loses three molecules of water. The next step of thermal decomposition occurs between 120 and 140 °C and is characterized by endothermic effects due to melting of the sample and further loss (35.5%) in weight. This loss corresponds to the abstraction of two 1-allylimidazole molecules, to give a compound of composition $[PdL_2Cl_2]$. In the FIR spectrum, a new band appears at 342 cm^{-1}, characteristic for Pd–Cl bonds. The presence of a single band shows the complex to be a *trans* isomer. Thus, the complex *trans*-$[PdL_2Cl_2]$ (**2**) was obtained by thermal degradation of complex **1** at 120 °C. The resulting solid was crystallized from acetone–toluene (1:1 v/v) to give complex **2** in the form of colourless crystals. Elemental analysis was in agreement with the formula $[PdL_2Cl_2]$ (Found: C, 36.6; H, 4.3; N, 14.3%. $C_{12}H_{16}Cl_2N_4Pd$ requires C, 36.62; H, 4.10; N, 14.23%).

2.2. X-ray crystallography

The X-ray intensity data of **1** and **2** were collected on a KM-4-CCD automatic diffractometer equipped with CCD detector, 30 s exposure time was used and all reflections of the Ewald sphere were collected up to $2\theta = 25°$. The unit cell parameters were determined from least-squares refinement of the setting angles of 5623 and 4529 strongest reflections, respectively, for **1** and **2**. Details concerning crystal data and refinement are given in Table 1. Lorentz, polarization and numerical absorption corrections [10] were applied. The structures were solved by the Patterson method and subsequently completed by difference Fourier recycling. All the non-hydrogen atoms were refined anisotropically using the full-matrix, least-squares technique. The hydrogen atoms were found by difference Fourier synthesis and they were refined as ''riding'' on their parent atoms and assigned isotropic temperature factors equal to 1.2 and 1.5 times the value of the equivalent temperature factor of the parent carbon or oxygen atom, respectively.

Table 1
Crystal data and structure refinement for complexes $[PdL_4]Cl_2 \cdot 3H_2O$ (**1**) and $[PdL_2Cl_2]$ (**2**)

	$[PdL_4]Cl_2 \cdot 3H_2O$ (**1**)	$[PdL_2Cl_2]$ (**2**)
Empirical formula	$C_{24}H_{38}Cl_2N_8O_3Pd$	$C_{12}H_{16}Cl_2N_4Pd$
Molecular weight	663.92	393.59
Temperature (K)	293(2)	100(1)
Radiation	Mo Kα ($\lambda = 0.71073$ Å)	Mo Kα ($\lambda = 0.71073$ Å)
Crystal system	Monoclinic	Triclinic
Space group	$C2/c$ (No. 15)	$P\bar{1}$ (No. 2)
a (Å)	17.8676(12)	5.170(2)
b (Å)	9.4915(14)	7.176(2)
c (Å)	19.1363(12)	10.308(2)
α (°)	–	93.59(3)
β (°)	105.596(6)	98.78(3)
γ (°)	–	93.37(3)
V (Å^3)	3125.8(5)	376.3(3)
Z	4	1
μ (mm^{-1})	0.809	1.579
Reflections collected	15,944	2257
Independent reflections (R_{int})	2776 (0.0269)	1464 (0.0294)
Final R_1, wR_2 [$I > 2\sigma(I)$]	0.0298, 0.0704	0.0276, 0.0732
Final R_1, wR_2 (all data)	0.0348, 0.0733	0.0277, 0.0733
Largest difference in peak and hole (e A^{-3})	0.382 and −0.366	1.751 and −1.397

The SHELXS97 [11], SHELXL97 [12] and SHELXTL [13] programs were used for all the calculations. Atomic scattering factors were those incorporated in the computer programs. The crystal data and details of data collection, together with the refinement procedure, are presented in Table 1.

2.3. NMR measurements

Solution-state NMR spectra were recorded on a Bruker Avance DRX 500 spectrometer operating at 500.13 MHz for ^{1}H, 125.258 MHz for ^{13}C and 50.664 MHz for ^{15}N. The chemical shift of acetone-d_6 signal (methyl groups) was used as a reference (δ_H 2.05 ppm; δ_C 30.5 ppm). For ^{15}N NMR, the nitromethane signal was used as an external standard for the chemical shift. The spectrometer was equipped with a pulse field gradient unit (50 G cm^{-1}). Five milligrams of samples were dissolved in 0.5 ml of the solvent for ^{13}C and 2D spectra while ^{1}H spectra were recorded at 5-fold lower concentrations. The ^{15}N signals were recorded with 2D Hetero Multi-Bond Correlation (HMBC) experiment, taking advantage of the Pulse Field Gradient (PFG) system and inverse detection [14]. The value of the sorting delay was set to 17 Hz, which allowed us to see geminal and vicinal ^{1}H–^{15}N *J*-couplings.

Sample **1** was observed only at low temperature. The ^{13}C NMR chemical shifts (in ppm) of **1** in acetone-d_6 at 193 K are: C1 = 138.52, C2 = 119.58, C3 = 129.00, C4 = 50.53, C5 = 131.75, C6 = 119.84. The ^{1}H NMR parameters for **1** (in acetone-d_6, ppm) are: H1 = 8.75, H2 = 6.77, H3 = 7.54, H4/H5 = 4.54, H6 = 5.77, H7 = 5.18, H8 = 5.06. The ^{15}N chemical shifts (ppm) are: N1 = 168.7, N2 = 177.2. For sample **2** (at 298 K, acetone-d_6, in ppm) are: C1 = 138.6, C2 = 118.5, C3 = 129.6, C4 = 50.4, C5 = 131.3, C6 = 119.7; H1 = 8.02, H2 = 6.85, H3 = 7.37, H4/H5 = 4.55, H6 = 5.93, H7 = 5.32, H8 = 5.25; N1 = 163.1, N2 = 174.2.

The solid-state CP MAS ^{13}C NMR experiments were performed on a Bruker Avance DSX 300 spectrometer at 75.47 MHz frequency, equipped with an MAS probehead using 4 mm ZrO_2 rotors. The conventional spectra were recorded with a proton 90° pulse length of 3.5 μs and a contact time of 1 ms. The repetition delay was 10 s and the spectral width was 25 kHz. The FIDs were accumulated with a time domain size of 4 K data points. The RAMP shape pulse was used during cross-polarization [15] and TPPM with τ_p 6.8 μs and a phase angle of 20° during the acquisition [16]. The cross-polarization efficiency was measured with contact times between 10 μs and 12 ms. The spectral data were processed using the WIN-NMR program [17]. A sample of glycine was used for setting the Hartmann–Hahn condition and a sample of adamantane was used as the chemical shift reference.

The PASS-2D experiment was carried out according to the procedure reported by Anzutkin et al. [18]. A detailed explanation of the PASS-2D pulse sequence and its performance, a *Mathematica* routine to generate a set of PASS solutions and the data processing can be found elsewhere [19,20].

2.4. Theoretical calculation

Calculations were carried out with the GAUSSIAN 98 program running on a Silicon Graphics Power Challenge computer [21]. The GIAO method with the B3PW91 hybrid method and 6-311G** and LanL2Dz basis set was used to calculate the NMR parameters.

3. Results

3.1. X-ray structures of complexes $[PdL_4]Cl_2 \cdot 3H_2O$ (1) and trans-$[PdL_2Cl_2]$ (2)

The structural arrangement and atom numbering system used are shown in Figs. 1 and 2 for complexes **1** and **2**, respectively. Selected bond angles, bond lengths and hydrogen bonds are given in Table 2.

In complex **1**, the immediate environment of the central atom is made up of the nitrogen atoms N(1), N(1a), N(11) and N(11a) of four imidazole rings. The molecule of **1**occupies two asymmetric units. The Pd(1) atoms lie on an inversion centre and the O(1) atoms lie on a 2-fold rotation axis (respectively, special positions *a* and *e* of the *C*2/*c* space group at 0, 0, 0 and 0, *y*, 1/4). The rest of the atoms lie in general positions. The coordination environment of the central ion has square-planar symmetry with Pd–N bond lengths of 2.017(2) and 2.019(2) Å. These distance are close to 2.0233(9) Å, the mean value determined for all Pd complexes possessing four nitrogen atoms in the coordination sphere found in CSD v 5.26 to be planar within the range of experimental error (the values can be described by the Gaussian distribution; checking statistics: median = 2.024, mode = 2.022, sampling variance = 0.0020, kurtosis = 31.09 and skewness = 0.251) [22]. In the coordinated *N*-allylimidazole molecules, both the bond lengths and the angles between the bonds are the same as those in other complexes of this azole [23–25]. The chloride anions appear outside the inner coordination sphere. They are situated on the symmetry axis of the coordination plane at a 3.877(3) Å from the palladium(II) ion. The chloride ions are bound with water molecules by hydrogen bonding, in which the Cl atom acts as an acceptor (A) of hydrogen, whereas the oxygen atom of the water molecule is a donor (D) (Table 2c). In all allylimidazole ligands, the heterocyclic rings are planar within the range of experimental error. The dihedral angles between the coordination plane of palladium(II) and the imidazole rings are 56.66(9)° and 85.27(8)°, for ligands indicated by N(1) and N(11) atoms, respectively.

The molecule of compound **2** occupies two asymmetric units. The Pd(1) atoms lie on inversion centre (special positions a of $P\bar{1}$ space group at 0, 0, 0) and the rest of the atoms lie in general positions. In the coordination plane

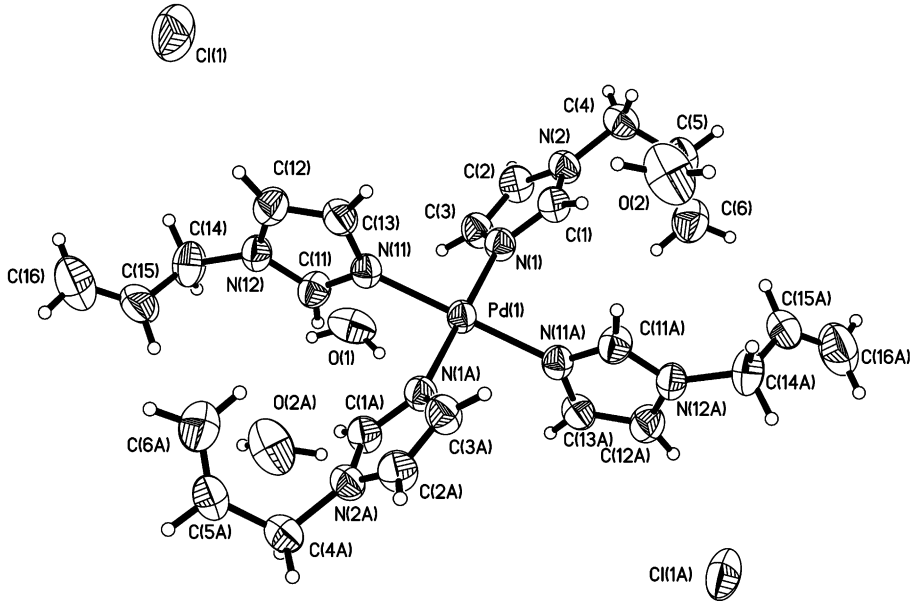

Fig. 1. The molecular structure of palladium(II) 1-allylimidazole complex $[PdL_4]Cl_2 \cdot 3H_2O$ (**1**).

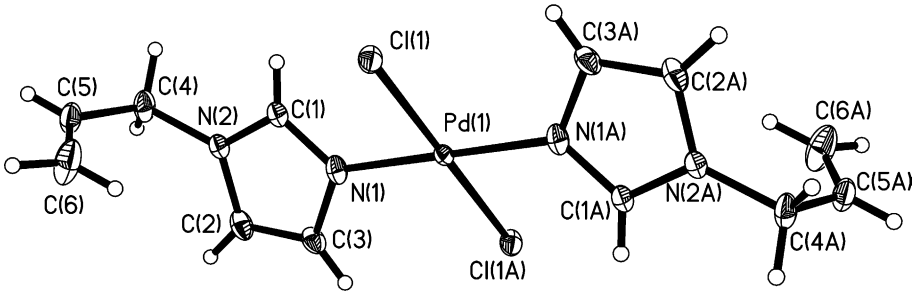

Fig. 2. The molecular structure of palladium(II) 1-allylimidazole complex *trans*-$[PdL_2Cl_2]$ (**2**).

of the square-planar symmetric complex **2**, two chloride ions and two nitrogen atoms of the imidazole rings occur in a trans relationship. The lengths of the Pd–Cl bonds are 2.306(2) Å and the lengths of the Pd–N bonds are 2.022(2) Å. These distance are close to 2.2966(7) and 2.033(1) Å, respectively, the mean values determined for all Pd complexes possessing two chlorine and two nitrogen atoms in the coordination sphere found in CSD v 5.26 to be planar within the range of experimental error (the values can be described by the Gaussian distribution; checking statistics, respectively: medians = 2.298 and 2.024, modes = 2.299 and 2.024, sampling variance = 0.00055 and 0.0011, kurtosis = 64.30 and 4.752, skewness = −4.447 and 0.8839) [22]. The latter are almost the same in length as those in compound **1**. The angles between the N(1)–Pd–N(1) and Cl–Pd–Cl bonds are 180° each, while those in *cis* position deviate by 0.4° from a right angle [90.4(1)° and 89.6(1)°]. The angles between the coordination plane and that formed by five atoms of the imidazole rings are 32.60(1)° each.

Table 2a
Selected bond lengths (Å) for complexes **1** and **2**

1				**2**	
Pd(1)–N(1)	2.019(2)	Pd(1)–N(11)	2.017(2)	Pd(1)–N(1)	2.022(2)
N(1)–C(1)	1.322(3)	N(11)–C(11)	1.322(3)	Pd(1)–Cl(1)	2.306(1)
N(1)–C(3)	1.384(3)	N(11)–C(13)	1.374(3)	N(1)–C(1)	1.318(4)
N(2)–C(1)	1.341(3)	N(12)–C(11)	1.335(3)	N(1)–C(3)	1.388(3)
N(2)–C(2)	1.374(3)	N(12)–C(12)	1.364(3)	N(2)–C(1)	1.344(4)
N(2)–C(4)	1.465(3)	N(12)–C(14)	1.477(3)	N(2)–C(2)	1.379(4)
C(2)–C(3)	1.350(3)	C(12)–C(13)	1.348(3)	N(2)–C(4)	1.466(4)
C(4)–C(5)	1.494(4)	C(14)–C(15)	1.481(4)	C(2)–C(3)	1.359(4)
C(5)–C(6)	1.293(4)	C(15)–C(16)	1.287(5)	C(4)–C(5)	1.500(4)
				C(5)–C(6)	1.308(5)

Table 2b
Selected bond angles (°) for complexes **1** and **2**

1				**2**	
N(11)–Pd(1)–N(1#1)	89.01(8)	N(11)–Pd(1)–N(1)	90.99(8)	N(1#1)–Pd–Cl	90.4(1)
				N(1)–Pd–Cl	89.6(1)
C(1)–N(1)–C(3)	106.47(19)	C(11)–N(11)–C(13)	106.2(2)	C(1)–N(1)–C(3)	107.0(2)
C(1)–N(2)–C(2)	107.3(2)	C(11)–N(12)–C(12)	107.5(2)	C(1)–N(2)–C(2)	107.1(2)
C(1)–N(2)–C(4)	125.6(2)	C(11)–N(12)–C(14)	126.0(2)	C(1)–N(2)–C(4)	125.9(3)
C(2)–N(2)–C(4)	126.9(2)	C(12)–N(12)–C(14)	126.3(2)	C(2)–N(2)–C(4)	126.8(2)
N(1)–C(1)–N(2)	110.7(2)	N(11)–C(11)–N(12)	110.6(2)	N(1)–C(1)–N(2)	110.9(2)
C(3)–C(2)–N(2)	107.0(2)	C(13)–C(12)–N(12)	106.8(2)	C(3)–C(2)–N(2)	107.2(2)
C(2)–C(3)–N(1)	108.5(2)	C(12)–C(13)–N(11)	108.8(2)	C(2)–C(3)–N(1)	107.9(3)
N(2)–C(4)–C(5)	113.3(2)	N(12)–C(14)–C(15)	110.8(2)	N(2)–C(4)–C(5)	113.3(2)
C(6)–C(5)–C(4)	127.2(3)	C(16)–C(15)–C(14)	125.5(3)	C(6)–C(5)–C(4)	126.2(3)

Symmetry transformations used to generate equivalent atoms: #1 $-x$, $-y$, $-z$.

Table 2c
Hydrogen bond lengths (Å) and bond angles (°) for complex **1**

D–H···A	D–H	H···A	D···A	DHA
O(1)–H(1O)···Cl(1)#1	0.90	2.38	3.247(2)	161.3
O(2)–H(2O)···Cl(1)#2	1.02	2.16	3.164(3)	168.1
O(2)–H(2P)···Cl(1)#3	0.89	2.45	3.219(3)	146.2

Symmetry transformations used to generate equivalent atoms: #1 $-x+0.5$, $y-0.5$, $-z+0.5$; #2 $-x+0.5$, $-y+0.5$, $-z$; #3 $x-0.5$, $-y+0.5$, $z-0.5$.

3.2. Low temperature NMR studies of *1* in solution

The apparent instability of **1** in the liquid phase prompted us to find the conditions which allow the observation of four allylimidazole ligands bonded to palladium. Low temperature measurements were found to be the method of choice. With a decrease of temperature, the yield of **1** gradually increased. At 263 K, ca. 10% of **1** is observed. The relative changes of both complexes are shown in pictorial form in Fig. 3. As seen, at 193 K, only complex **1** is observed. It is worth noting the high diagnostic value of the chemical shift of the H1 proton, which is most sensitive to coordination. The low temperature ^{15}N measurements provided further evidence which confirms the presence of **1** at 193 K. Very similar results were obtained in both acetone-d_6 and methylene chloride-d_2. The process of formation of **1** is reversible. The $\ln K$ values are 2.38, 0.48, −3.51 and −5.24 at temperatures of 283, 263, 233 and 223 K, respectively.

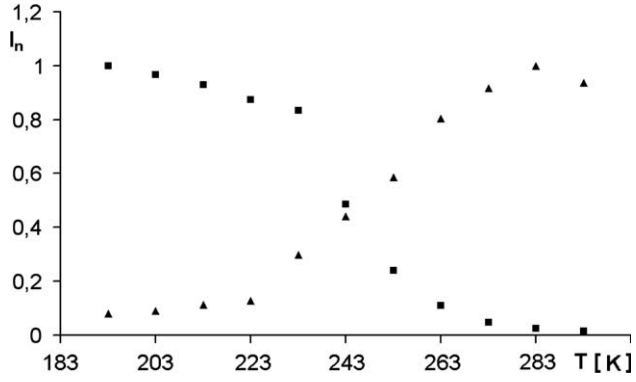

Fig. 3. Change of proportion of **1** versus **2** as a function of temperature. The filled triangles denote sample **2** while filled squares denote sample **1**.

3.3. NMR studies in the solid phase

3.3.1. Analysis of ^{13}C isotropic values

Fig. 4(a) shows the ^{13}C CP MAS spectrum of **2** recorded at room temperature with a spinning speed of 8 kHz. The detailed analysis of the isotropic chemical shifts and comparison of data in both phases allows us to note significant differences. In the liquid phase, signals corresponding to the C(2) and C(6) atoms are very close to each other and appear at ca. 120 ppm, while in the solid phase, these resonances are separated by 8 ppm. It is not evident which signal represents the allylic part of **2**. In order to clarify the assignment for **2**, we used the Lee–Goldburg decoupling experiment (LGD) [26]. In this technique, the ^{1}H homonuclear dipole–dipole couplings are removed while the *J*-couplings between carbon and proton can be observed. In the case of **2**, we should observe triplets for C4 and C6 and doublets for the other carbons. Fig. 4(b) presents the spectrum of **2** in the region of interest. Although the lines are broadened, mostly due to the quadrupolar effect of ^{14}N, ^{35}Cl and ^{37}Cl, the doublet of C(2) (121.5 ppm) and the triplet of C(6) (113.5 ppm) provide equivocal proof which allows us to assign the resonance lines to the structure. Our results show that the LGD experiment can be an important alternative approach to other commonly used spectral editing techniques [27].

As in the previous case, the ^{13}C isotropic chemical shifts values for sample **1** were obtained by performing the CP/MAS experiment with sample spinning of 8 kHz. Inspection of the ^{13}C δ_{iso} values unambiguously proves that the

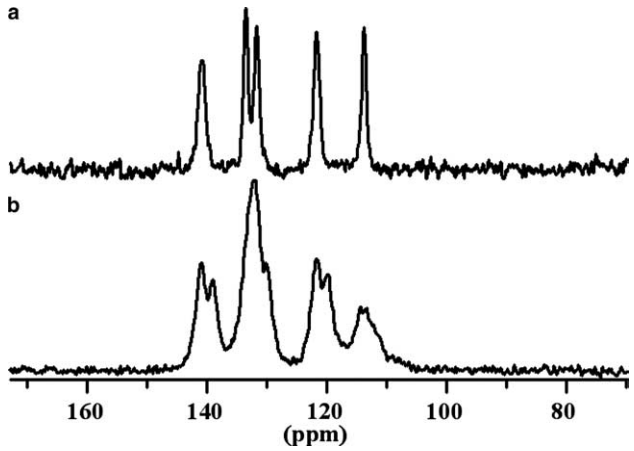

Fig. 4. (a) 75.46 MHz ^{1}H–^{13}C CP MAS spectra of **2** recorded at 8 kHz MAS with RAMP shape cross-polarization and TPPM decoupling. (b) Spectrum of **2** with Lee–Goldburg decoupling. The spectra have 4096 data points with 20 Hz line broadening.

bulk material under investigation contains only pure complex **1**. The assignment of signals for **1** was done using comparative analysis with the NMR dataset for complex **2.** The X-ray data (Section 3.1) clearly shows that, for **1**, two conformations of the allylic fragment with respect to the imidazole ring exist, one with the N12–C(14)–C(15)–C(16) torsional angle equal to 123.50° (gauche) and the second with the N(2)–C(4)–C(25)–C(6) angle equal to 5.30° (*syn*). The corresponding angle for complex **2** is equal to 0.09°. Taking into account the geometry of the allylic chain obtained by X-ray diffraction for both samples and the NMR chemical shifts in the solid state, we were in a position to assign all the ^{13}C signals (Table 3). The difference between the δ_{iso} of C6 and C16 allylic carbons of **1** is 5.6 ppm. In the folded geometry, the distance between C(6) and C(1)/C(2) carbons of the imidazole ring is 3.32 and 3.62 Å, respectively. The analogous distances for C(16) are 3.95 and 4.58 Å. In the folded conformation, the ring current effect influences the shielding of C(16) carbon and causes its upfield shift.

3.3.2. Analysis of ^{13}C chemical shift anisotropy

Going further into the NMR analysis of complexes **1** and **2**, we were attracted by the prospect of analysing the ^{13}C δ_{ii} data for both compounds and of inspecting the anisotropic values (CSAs) of the chemical shift tensors (CST). Knowledge of these parameters allows us to analyse in detail the electronic surroundings for each carbon and, furthermore, their correlation to molecular structure [28].

Fig. 5(a) shows the ^{13}C CP MAS experimental spectrum of **2**, recorded with a spinning rate of 1.8 kHz. The calculated spectrum, employing the graphical method of Herzfeld–Berger, is displayed in Fig. 5(b) [29]. The ^{13}C δ_{ii} elements used for calculation of spectrum 5b and other NMR shielding parameters [span (Ω) and skew (κ)] are given in Table 3.

Analysis of the span parameters leads to interesting conclusions. Evidently, we have two sets of Ω: the first ca. 143 ppm and the second ca. 190 ppm. The first one characterizes imidazole carbons, while the second represents an allylic fragment. Thus, the anisotropic values provide additional proof which enabled us to assign signals to the structure.

The comparison of ^{13}C δ_{ii} parameters for **1** and **2** is a challenging question. However, in the case of **1**, which consists of 12 carbon atoms (Fig. 6(a)), the deconvolution procedure is not an easy task. At low spinning speed (Fig. 6(b)), an overlap between different spinning sidebands manifolds occurs and analysis of the spectrum is ambiguous. Separation of the isotropic and anisotropic parts of the spectra with heavily overlapping systems is still a challenge for solid-state NMR spectroscopy. There are several

Table 3
Experimental chemical shift parameters ^{13}C δ_{ii} and corresponding anisotropic parameters for **1** and **2**

Compound	Carbon atom	δ_{iso} (ppm)	δ_{11} (ppm)	δ_{22} (ppm)	δ_{33} (ppm)	Ω (ppm)	κ
2	C(1)	140.6	201	147	74	127	0.15
	C(2)	121.5	186	118	59	127	−0.09
	C(3)	131.6	202	133	59	143	0.03
	C(4)	49.5					
	C(5)	133.3	232	124	44	188	−0.15
	C(6)	113.5	213	107	21	192	−0.10
1	C(1)	139.5	207	145	69	138	0.12
	C(11)	137.9	205	140	70	135	0.05
	C(2)	120.8	194	120	52	142	−0.02
	C(12)	120.8	194	120	52	142	−0.02
	C(3)	131.7	204	133	60	144	0.03
	C(13)	128.5	201	128	58	143	−0.01
	C(4)	49.6					
	C(14)	45.2					
	C(5)	133.9	233	130	40	193	−0.06
	C(15)	133.2	232	125	46	186	−0.13
	C(6)	114.3	216	106	22	194	−0.13
	C(16)	119.9	209	117	36	173	−0.05

Estimated errors in δ_{11}, δ_{22}, δ_{33} are ±3 ppm; span is expressed as $\Omega = \delta_{11} - \delta_{33}$, skew as $\kappa = 3(\delta_{22} - \delta_{iso})/\Omega$.

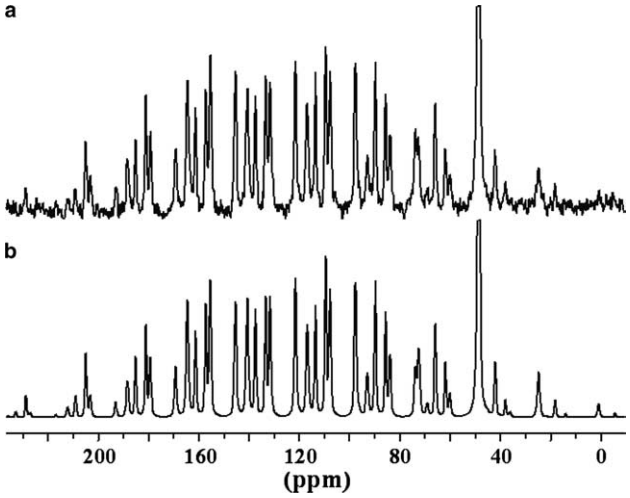

Fig. 5. (a) 75.46 MHz ^{1}H–^{13}C CP MAS spectra of **2** recorded at 1.8 kHz with TPPM decoupling. (b) Spectrum simulated with a WINMAS program. The spectra have 4096 data points with 20 Hz line broadening.

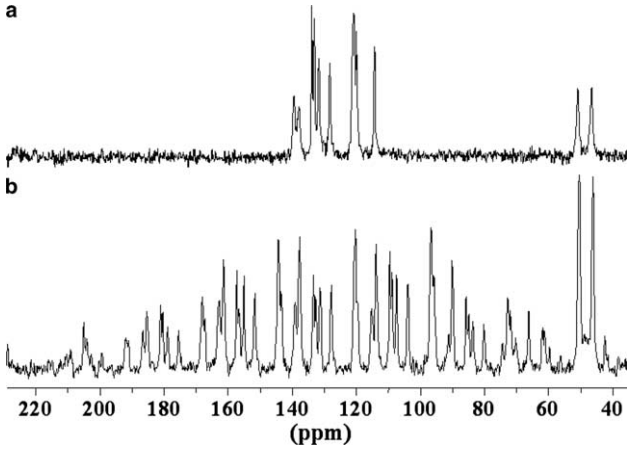

Fig. 6. 75.46 MHz ^{1}H–^{13}C CP MAS spectra of **1** recorded at 8 kHz MAS with RAMP shape cross-polarization and TPPM decoupling (a), and at 1.8 kHz with CP and TPPM decoupling (b). The spectra have 4096 data points with 20 Hz line broadening.

approaches which allow us to achieve this goal. Recently, Antzutkin et al. introduced the PASS 2D sequence [18,19] which, compared to previous techniques, offers good sensitivity and does not require any hardware modifications or any special probehead.

Fig. 7(a) displays the PASS-2D spectrum of **1**, recorded with a spinning rate of 1.8 kHz. By proper data shearing (Fig. 7(b)) it is possible to separate spinning sidebands for each carbon and to employ a calculation procedure in order to establish the ^{13}C δ_{ii} parameters. The experimental and the best-fitting simulated 1D spinning CSA sideband pattern for carbons of **1** are shown in Fig. 8. The sidebands are clear-cut and easy to analyse. The imidazole ring signals are well separated and the intensity of sidebands can be established. The anisotropy of the allylic carbons is largest compared to other resonances, consistent with the data recorded for **2**. Having such information, we were in a position to establish ^{13}C δ_{ii} parameters for **1** (Table 3).

The ^{13}C CST parameters and Ω values indicate that, for both molecules, a distortion of geometry of the allylic part is larger than that for imidazole carbons. The skew parameter (κ) close to zero means that, for all carbon atoms, the shielding is not localized to a particular bond but is averaged out over the entire environment.

3.3.3. Theoretical calculations of ^{13}C chemical shift tensor parameters

A number of methods are currently available for computing NMR parameters [30,31]. In our calculations, we have used coordinates taken from X-ray measurements as an input file. The advantage of such an approach is related to the fact that it is possible to compare the theoretical and experimental results for molecules with exactly the same geometry of heavy atoms. One of the most important steps in the case of metal complexes are the choice of the proper basis set. In the first approach for calculation of the ^{13}C

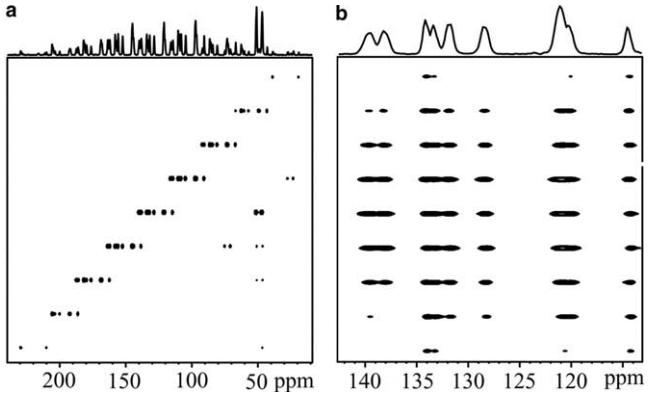

Fig. 7. (a) PASS-2D spectrum of **1** recorded with a spinning rate of 1.8 kHz. (b) Tilted spectrum a.

NMR shielding parameters of **1** and **2** employing the GAUSSIAN program, we have used the GIAO B3PW91 hybrid method, the LanL2Dz basis set on palladium and 6-311G** basis set on other atoms. Unfortunately, the correlation between calculated and experimental ^{13}C isotropic chemical shifts was very bad, as shown in the number of scatter points [32]. Much better results were obtained when the LanL2Dz basis set was applied for each atom. Calculated shielding parameters are attached as Supplementary material. The comparison of experimental and calculated parameters shows a very good correlation and confirmed the assignment of the NMR signals to the molecular structure [32]. In particular, this approach is valuable for sample **1** with different orientation of allyl residues bonded with imidazole. Without doubt, it is possible to distinguish the folded and unfolded geometries of the allyl groups. The analysis of calculated ^{13}C δ_{ii} versus experimental ^{13}C δ_{ii} is very diagnostic [32].

The comparison of experimental and theoretical span parameters, defined as $\Omega = \delta_{11} - \delta_{33}$, is a source

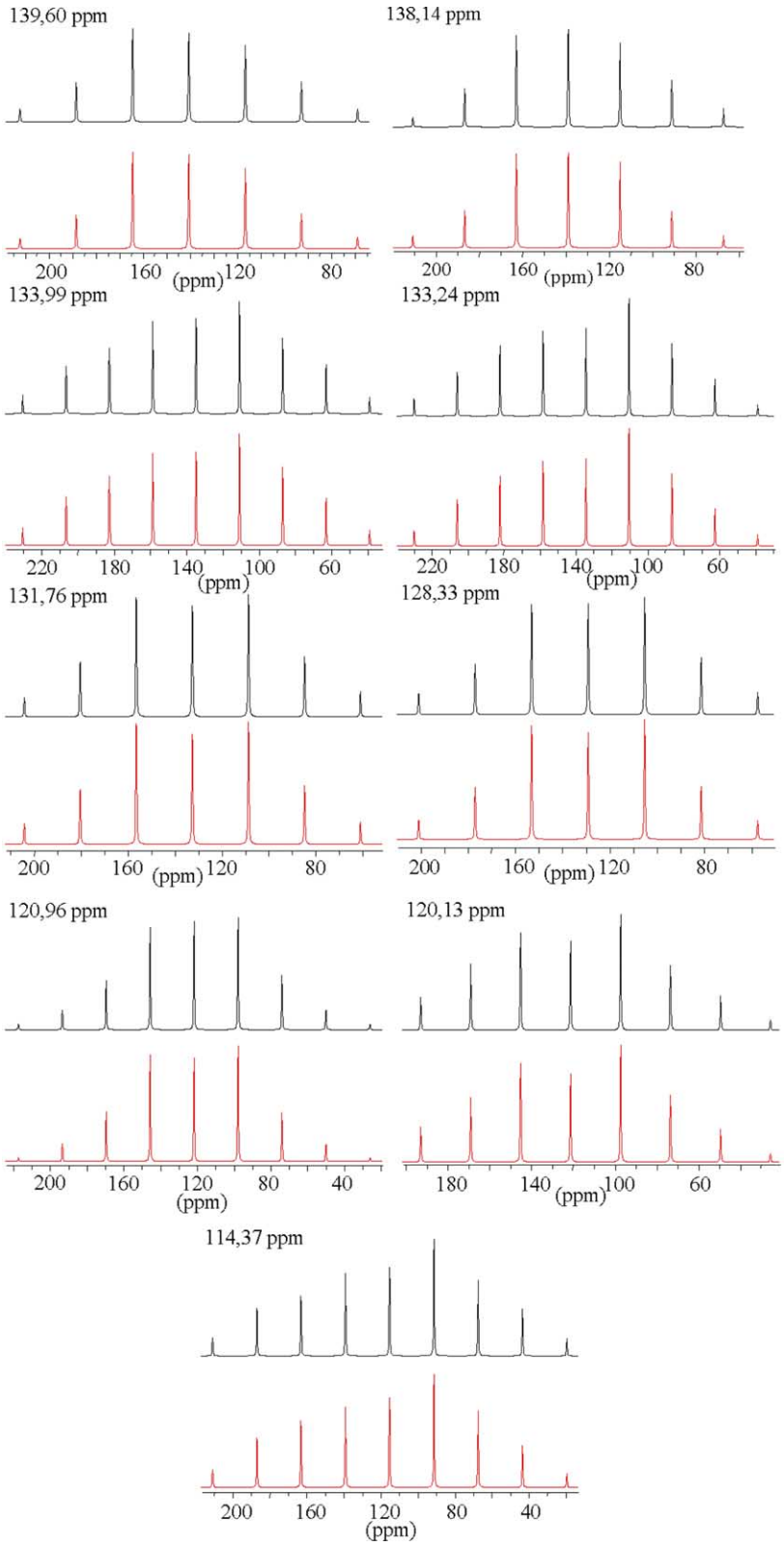

Fig. 8. The experimental and best fitting simulated 1D spinning CSA sideband pattern for selected carbons of **1**.

of interesting information about molecular dynamics [32]. It is worth noting that, for both complexes, the correlation of Ω_{exp} to Ω_{theo} is much better for the allyl group in a folded conformation. For the unfolded geometry, minute scatter of the experimental points is seen. Such observations suggest small amplitude motion of unfolded allylic fragment in the crystal lattice while the folded part is very rigid.

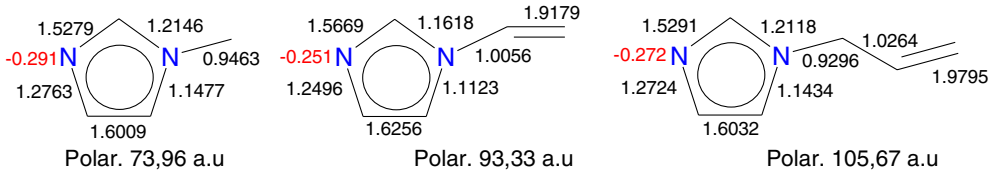

Fig. 9. Calculated values of electron density, bond orders and polarizability for methyl-imidazole, vinyl-imidazole and allyl-imidazole.

4. Discussion

Our NMR data shows that in the liquid state, the Pd(II) complex with four allyl-imidazole ligands is unstable and can exist only under special conditions (low temperature) whilst in the solid phase, $[PdL_4]Cl_2$ sample is relatively stable. The fact that the process of Pd–N bond breaking can be brought under control may have practical implications and can be a subject of potential interest, especially in relation to catalytic processes.

It is well known that formation and stability of complexes depends on a few factors which characterize the physico-chemical properties of ligands; e.g., basicity, nucleophilicity, electron density distribution, steric effects, etc. The basicity of imidazole derivatives and its influence on the stability of complexes with metals (Co^{II}, Ni^{II} and Cu^{II}) was exhaustively discussed in our previous paper [25]. In this part of the project, we were prompted to compare the electronic properties of allyl-imidazole ligand with other small imidazole derivatives such as methyl-imidazole and vinyl-imidazole. Some of structural parameters can be obtained by employing a theoretical approach. Employing DFT theoretical calculation with the B3PW91 functional and 6-311++G** basis set, we established the electron density on each atom, the bond orders and polarizability. The obtained values are shown in Fig. 9.

Comparing the three molecules under discussion, the most significant differences are noted for the electron density on the N3 nitrogen and the polarizability. It is worth noting that the bond order parameters for methyl-imidazole and allyl-imidazole are comparable. Moreover, methyl-imidazole is the species with the largest electron density. If the tendency to form Pd···N bonds is related to the electron density on the N3 atom, adding methyl-imidazole to sample **1** or **2** should lead to ligand exchange. In fact, such a process was observed. Addition of a stoichiometric amount of methyl-imidazole to a flask containing complex **1** or **2** leads immediately to the formation of a new complex, insoluble in acetone and methylene chloride. Its molecular structure was confirmed by ^{13}C solid-state NMR and MALDI-TOF MS [32].

A challenging question, which is important to understanding the mechanism of ligand exchange, is the role of water and hydrogen bonding with the chloride anion. As stated in Section 3.1, for sample **1**, chloride ions are outside the inner coordination sphere in the crystal lattice. In the liquid phase, due to solvation effects, the strength of hydrogen bonding between chloride and water may be significantly different. Released chloride ions can replace allyl-imidazole in structure **1**, leading to the formation of complex **2**. The low temperature stabilizes the hydrogen bonded complex formed by water and chloride, allowing the allyl-imidazole ligand to bond and the formation of complex **1**. This process is reversible and depends on the applied experimental conditions.

5. Conclusions

In this work, comparative, structural studies in solution and in the solid state of two palladium(II) complexes with different numbers of *N*-allyl-imidazole ligands were carried out, employing a multi-technique approach. Our investigations clearly proved that, in solution, the complex with four allyl-imidazole ligands is unstable at room temperature and can be observed only at low temperatures. 1D Lee–Goldburg decoupling and 2D PASS experiments were used to assign the structure in the solid phase. To the best of our knowledge, this report shows the first application of PASS-2D technique in structural studies of metal complexes. In particular, this method can be valuable in the analysis of insoluble complexes.

Acknowledgements

S. Olejniczak is grateful to the Foundation for Polish Science for the scholarship "Domestic Grants for Young Scientists". The authors are indebted to Dr. Colan E. Hughes (Cardiff University) for proof reading the manuscript.

Appendix A. Supplementary data

Tables of crystal data and structure refinement, anisotropic displacement coefficients, atomic coordinates and equivalent isotropic displacement parameters for non-hydrogen atoms, H-atom coordinates and isotropic displacement parameters, bond lengths and interbond angles have been deposited with the Cambridge Crystallographic Data Centre under No. CCDC146012 and CCDC146013 for compounds **1** and **2**, respectively. Copies of this information may be obtained free of charge from The Director, CCDC, 12 Union Road, Cambridge, CB2 1EZ, UK (fax: +44 1223 336033; e-mail: deposit@ccdc.cam.ac.uk or http://www.ccdc.cam.ac.uk).

Calculated NMR shielding parameters as well figures showing correlations between theoretical and experimental data are attached. Supplementary data associated with this

article can be found, in the online version, at doi:10.1016/j.jorganchem.2005.10.045.

References

[1] A. Togni, L.M. Venanzi, Angew. Chem., Int. Ed. 33 (1994) 497–526.
[2] (a) G.A. Grasa, A.C. Hillier, S.P. Nolan, Org. Lett. 3 (2001) 1077–1080;
(b) A.S. Abu-Surrah, M. Kettunen, K. Lappalainen, U. Piironen, M. Klinga, M. Leskelä, Polyhedron 21 (2002) 27–31.
[3] C. Mazet, L.H. Gade, Organometallics 20 (2001) 4144–4166.
[4] (a) M.R. Buchmeiser, Th. Schareina, R. Kempe, K. Wurst, J. Organomet. Chem. 634/1 (2001) 39–46;
(b) J. Silberg, T. Schareina, R. Kempe, K. Wurst, M.R. Buchmeiser, J. Organomet. Chem. 622 (2001) 6–18;
(c) M.R. Buchmeiser, K. Wurst, J. Am. Chem. Soc. 121 (1999) 11101–11107.
[5] D.J. Nielsen, K.J. Cavell, B.W. Skelton, A.H. White, Organometallics 20 (2001) 995–1000.
[6] M.C. Done, T. Ruether, K.J. Cavell, M. Kilner, E.J. Peacock, N. Braussaud, B.W. Skelton, A.H. White, J. Organometal. Chem. 607 (2000) 78–92.
[7] K.R. Reddy, G.G. Krishna, Tetrahedron Lett. 46 (2005) 661–663.
[8] C.J. Mathews, P.J. Smith, T. Welton, J. Mol. Catal. Chem. 206 (2003) 77–82.
[9] F.E. Hahn, B. Heidrich, T. Lugger, T. Pape, Z. Naturforsch. B 59 (2004) 1519–1523.
[10] STOE & Cie, X-RED, Version 1.18. STOE & Cie GmbH, Darmstadt, Germany, 1999.
[11] G.M. Sheldrick, Acta Crystallogr. A46 (1990) 467–473, and references cited therein.
[12] G.M. Sheldrick, SHELX97, Program for the Solution of Crystal Structures, University of Göttingen, Germany, 1997.
[13] G.M. Sheldrick, SHELXTL: Release 4.1 for Siemens Crystallographic Research Systems, 1990.
[14] S. Berger, S. Braun, in: 200 and More NMR Experiments, A Practical Course, Wiley-VCH Verlag-GmbH, CoKGaA, Weinheim, 2004.
[15] G. Metz, X. Wu, S.O. Smith, J. Magn. Reson. A 110 (1994) 219–227.
[16] A.E. Bennet, C.M. Rienstra, M. Auger, K.V. Lakashmi, R.G. Griffin, J. Chem. Phys. 103 (1995) 6951–6958.
[17] WIN-NMR, Bruker-Franzen Analytik GmbH, Version 6.0, Bremen, Germany, 1993.
[18] O.N. Antzutkin, S.C. Shekar, M.H. Levitt, J. Magn. Reson. 115 (1995) 7–18.
[19] O.N. Antzutkin, Y.K. Lee, M.H. Levitt, J. Magn. Reson. 135 (1998) 144–152.
[20] O.N. Antzutkin, Prog. Nucl. Mag. Res. Sp. 35 (1999) 203–266.
[21] M.J. Frisch, G.W. Trucks, H.B. Schlegel, G.E. Scuseria, M.A. Robb, J.R. Cheeseman, V.G. Zakrzewski, J.A. Montgomery Jr., R.E. Stratmann, J.C. Burant, S. Dapprich, J.M. Millam, A.D. Daniels, K.N. Kudin, M.C. Strain, O. Farkas, J. Tomasi, V. Barone, M. Cossi, R. Cammi, B. Mennucci, C. Pomelli, C. Adamo, S. Clifford, J. Ochterski, G.A. Petersson, P.Y. Ayala, Q. Cui, K. Morokuma, D.K. Malick, A.D. Rabuck, K. Raghavachari, J.B. Foresman, J. Cioslowski, J.V. Ortiz, B.B. Stefanov, G. Liu, A. Liashenko, P. Piskorz, I. Komaromi, R. Gomperts, R.L. Martin, D.J. Fox, T. Keith, M.A. Al-Laham, C.Y. Peng, A. Nanayakkara, C. Gonzalez, M. Challacombe, P.M.W. Gill, B. Johnson, W. Chen, M.W. Wong, J.L. Andres, C. Gonzalez, M. Head-Gordon, E.S. Replogle, J.A. Pople, GAUSSIAN 98, Revision A.6, Gaussian, Inc., Pittsburgh, PA, 1998.
[22] The refcodes of analysed compounds are available from authors on request.
[23] K. Kurdziel, T. Głowiak, Pol. J. Chem. 72 (1998) 2181–2188.
[24] T. Głowiak, K. Kurdziel, J. Mol. Struct. 516 (2000) 1–5.
[25] K. Kurdziel, T. Głowiak, Polyhedron 19 (2000) 2183–2188.
[26] A. Bielecki, A.C. Kolbert, M.H. Levitt, Chem. Phys. Lett. 155 (1989) 341–346.
[27] K.W. Zilm, in: D.M. Grant, R.K. Harris (Eds.), Spectral Editing Techniques: Hydrocarbon Solids in Encyclopedia of NMR, vol. 7, Wiley, Chichester, 1996, pp. 4498–4503.
[28] W.S. Veeman, Prog. Nucl. Mag. Res. Sp. 16 (1984) 193–235.
[29] (a) J. Herzfeld, A. Berger, J. Chem. Phys. 73 (1980) 6021–6030;
(b) G. Jeschke, G. Grossmann, J. Magn. Reson. A 103 (1993) 323–328.
[30] D.M. Grant, J.C. Facelli, D.W. Alderman, M.H. Sherwood, in: J.A. Tossell (Ed.), Nuclear Magnetic Shielding and Molecular Structure, Kluwer, Academic Publishers, Dordrecht, 1993, pp. 367–384.
[31] M. Buhl, M. Kaupp, O.L. Malkina, V.G. Malkin, J. Comput. Chem. 20 (1999) 91–105.
[32] See Supplementary materials.